ADVANCED ENGINEERING MATERIALS

FULL PAPER

DOI: 10.1002/adem.201600012

Shape-Memory Topographies on Nickel–Titanium Alloys Trained by Embossing and Pulse Electrochemical Machining**

By *Mareike Frensemeier,* Dominik Schirra, Martin Weinmann, Olivier Weber* and *Elmar Kroner*

The two-way shape-memory effect (TWSME) in Nickel–titanium (NiTi) alloys is of interest for applications in aerospace, biomedicine, and microengineering due to its reversible shape recovery. In this study, the authors demonstrate two approaches to obtain switchable surface structures using the TWSME. Samples are structured using two surface geometries by either cold embossing, or pulse electrochemical machining (PECM). After planarization, a change from optically smooth to structured and vice versa is observed. The switch is induced through heating and cooling the sample above and below the phase transformation temperature. The protrusions reflect the pattern applied by the two processes. Both methods are promising for preparation of switchable metallic surfaces on larger areas.

1. Introduction

Nickel–titanium (NiTi) shape-memory alloys are capable of recovering their previously defined shape after certain deformation at temperatures above their characteristic transformation temperature. This shape change is due to the one-way shape-memory effect (OWSME), which has its origin in a martensitic phase transformation. If deformed in the martensitic phase, subsequent heating above the austenite start temperature leads to a shape recovery by the transformation back to austenite upon heating.[1] Due to a coordinated displacement in the atomic structure, a completely reversible deformation, even for large strains up to approximately 3–8%, can be induced.[2] By combining deformation processing and specific heat treatment, it is possible to induce an intrinsic two-way shape-memory effect (TWSME).[3,4] This effect allows a reversible shape change as a function of cycling temperature without external restoring force.

Studies by Zhang et al. have shown that a TWSME can be induced on a NiTi surface using an indentation method, which leads to switchable surface protrusions.[5–7] Near equiatomic NiTi samples were indented, heated above the transformation temperature, cooled down again, and then planarized by grinding and polishing. When the planarized sample was heated above the transformation temperature, protrusions formed on the sample surface and disappeared after the sample was cooled back to room temperature. This phenomenon was found to be repeatable over multiple temperature cycles. The protrusions were attributed to preferentially oriented dislocation structures in proximity to the former indentation site. We recently performed a microstructural study of Ti–50.9 at% Ni shape-memory surfaces after indentation and found both dislocations and thermally stabilized martensitic plates oriented along to the indents.[8] It was proposed that the stabilized martensite acts as a nucleation site for the TWSME and is crucial for inducing

[*] *M. Frensemeier, D. Schirra, Dr. E. Kroner*
INM – Leibniz Institute for New Materials, Campus D2 2, 66123 Saarbrücken, Germany
E-mail: mareike.frensemeier@leibniz-inm.de
M. Frensemeier, D. Schirra
Department of Materials Science and Engineering, Saarland University, Campus D2 2, 66123 Saarbrücken, Germany
Dr. M. Weinmann
Department of Physical Chemistry, Saarland University, Campus B2 2, 66123 Saarbrücken, Germany
Dr. O. Weber
Center for Mechatronics and Automatization, Gewerbepark Eschberger Weg, Geb. 9, 66121 Saarbrücken, Germany
Dr. O. Weber
Institute of Production Engineering, Saarland University, Campus A4 2, 66123 Saarbrücken, Germany

[**] *The authors thank the mechanical workshop of the INM for the tool fabrication. M. F. and E. K. gratefully acknowledge support of this work from the European Research Council, ERC Advanced Grant "Switch2Stick," Agreement No. 340929, awarded to E. Arzt. (Supporting Information is available online from Wiley Online Library or from the author).*

reversible surface protrusions. All these studies suggest that alloys with a TWSME are, in principle, able to reversibly change their surface topography as a function of temperature. As many physical properties depend on the surface structure of a material, a switchable surface geometry may be utilized to achieve a switchable functionality.

A TWSME surface with a reversible change from flat to a structured topography may lead to new applications in the field of tribology, in microfluidics, and in biomedical devices.[9–11] However, implementation and testing of new functionalities usually require larger surface areas. The conventional preparation technique via individual indents or scratches is time-consuming and difficult to scale up.[5] Liu et al. used a layer of packed soda lime glass balls to indent an array of holes simultaneously into a shape-memory polymer leading to an array of microprotrusions.[12] This cost and time-efficient method is limited to a spherical protrusion geometry. The use of machining methods such as drilling or milling, which would enable a variation in geometry and subsequently a well-defined shape change of the NiTi surface are challenging and would lead to high tool wear.[13,14] Due to a high degree of work hardening and their characteristic ductility, NiTi shape-memory alloys show high wear resistance and poor machinability.[13,15,16] Therefore, the purpose of this study is to expand the limited preparation techniques on TWSME surfaces in NiTi to methods which can be applied on larger scales and allow high localized deformation at the same time.

In this study, two plastic forming approaches are pursued to facilitate and optimize the preparation of surfaces with TWSME in a martensitic Ti–50.3 at% Ni alloy. In the first approach, the NiTi alloy is trained by cold embossing using a metallic micro-mesh as a template. The remaining deformation after embossing is removed by mechanical grinding. In the second approach, the NiTi alloy is pre-patterned using pulse electrochemical machining (PECM) and subsequent planarization via compression with a smooth work piece. The PECM process allows comparatively fast formation of stress-free surface structures with high accuracy and without generation of heat,[17] which is beneficial for large area training of the indentation induced TWSME of NiTi alloys.[18–20]

2. Experimental Section

2.1. Embossing

A polycrystalline NiTi shape-memory alloy composed of Ti–50.3 at.% Ni (Ti–55.47 wt.% Ni) was procured from Memry GmbH (Germany). The phase transformation temperatures were measured by differential scanning calorimetry (DSC) using a Mettler Toledo DSC1 Star System. The martensite finish temperature (M_f) is about 25 °C, and the austenite finish temperature (A_f) is about 76 °C. A two millimeter thick NiTi sheet was cut into pieces of 10×10 mm and discs of 10 mm diameter. The NiTi samples were ground using 2500 grade SiC paper, followed by several mechanical polishing steps down to 1 μm diamond paste, and oxide polishing with an OP-S suspension (Struers, Germany). The resulting average surface roughness (R_a) was 40 ± 6 nm, measured by white light interferometry (Zygo NewView 5000, Kyoto, Japan).

Cold embossing was performed in a hydraulic press (Paul-Otto-Weber GmbH) using a metallic micro-mesh. The cloth-like mesh was made from fine stainless steel wires, procured from Haver & Boecker (TRD 75) with a mesh size of 75 μm and cloth thickness of 260 μm, (Figure 1A). Three samples were embossed with at a load of 100 kN for 10 s. The samples were then planarized in two steps, using an optically smooth hard metal work piece and an active oxide suspension for polishing (OP-S Suspension, Struers, Germany) to regain an average roughness of 50 ± 5 nm.

2.2. Pulse Electrochemical Machining – PECM

The polished NiTi discs, representing the anode of the setup, were fixated in the flushing chamber of a PEM-Center8000 (PEMTec SNC, France). Two different tools, one with a pattern of grooves and one with holes as shown in Figure 1B, were prepared via drilling and milling from stainless steel and were used as a cathode. The faces of the two stainless steel tools had a diameter of 12 mm. The holes of 1 cm depth had diameters 150, 250, 500, and 1 000 μm; the size of the grooves was 120, 150, 250, and 500 μm at a depth of 250 μm. The electrolyte was axially fed up through a flushing chamber (Figure 2) so that uniform flushing conditions were obtained in the interelectrode gap, which was set at an initial size of 30 μm. A sodium nitrate ($NaNO_3$) electrolyte, with an electrical conductivity of 72 mS cm^{-1} at 21 °C and a pH value of 7.2, was pumped into the gap at a flow rate of 10 L min^{-1}

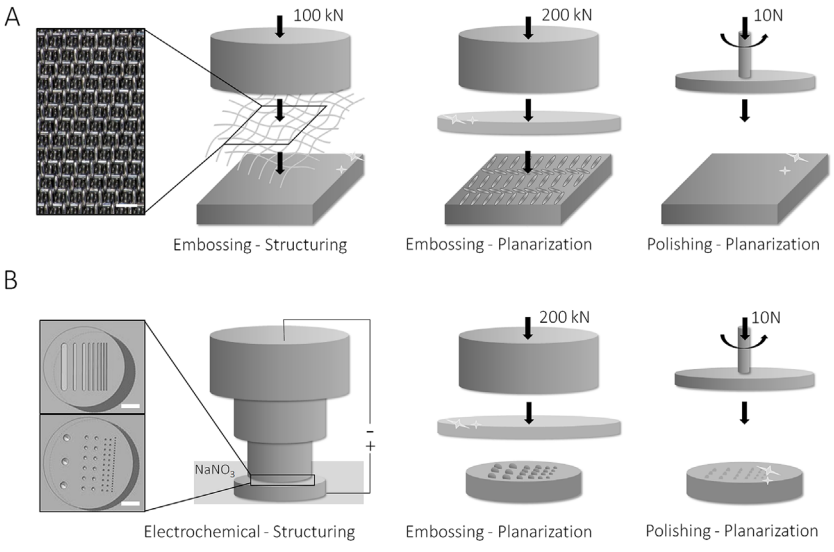

Fig. 1. Schematic of the two preparation techniques for shape-memory surfaces. (A) Cold embossing using a metallic micro-mesh, the result of which is demonstrated in the optical micrograph (inset, scale bar 200 μm). (B) Pulse electrochemical micromachining of a NiTi surface with two structured tools with grooves and with holes of different sizes (inset, scale bar 1 mm).

FULL PAPER

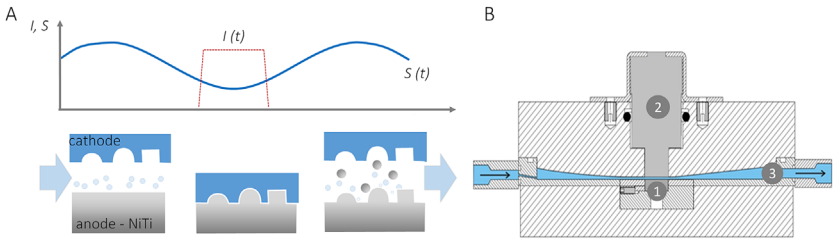

Fig. 2. Schematic drawing of the PECM process and resulting surface texture. (A) The cathode is moved in a sinusoidal manner to widen the interelectrode-gap (S, gap distance) to the anode. A short pulse (I, current pulse) is applied at the lower turning point. (B) Experimental PECM-Setup. 1: NiTi sample, 2: tool cathode, 3: electrolyte flow. Modified according to Weinmann and Zapp et al.[21,22]

and a pressure of 250 kPa. The amplitude of the cathode vibration was 373 μm. The applied voltage amplitude was set to 12.8 V, the electrical pulse on-time to 2.5 ms, the electrical and mechanical pulse frequencies to 50 Hz, and the cathode feed rate to 0.27 mm min^{-1}. The angular phase shift between the bottom dead center of the mechanical vibration and the triggering of the electrical current impulse was set to 0.65. During the machining process, the surface patterns of the cathode were negatively transferred to the anode.

The surface morphology of the PECM samples was analyzed by scanning electron microscopy using an FEI Versa 3D Dual Beam (Oregon, USA) microscope. Topography measurements were carried out by white-light interferometry in a 3-D optical microscope (Keyence, VHX 2000D, Japan).

Subsequently, the surface structures on the NiTi surface were compressed with the smooth hard metal work piece at a load of 200 kN. The remaining surface roughness was mechanically and chemically polished as described above for cold embossing.

The shape-memory behavior of both samples was investigated by thermal cycling and in situ characterization of the surface topography. Heating and cooling were conducted with a Peltier heating and cooling stage (Linkam, PE 120, UK), which was installed in the white light interferometer for in situ topography measurements. Experiments were made at room temperature (23 °C), at 80 °C, and again after cooling down to room temperature. The temperatures were chosen to be above and below the phase transformation temperatures of the alloy. White light interferometry images were taken after hold times of 1 min to ensure a homogenous temperature distribution. Thermal cycling was conducted over 10 times to measure the reversibility of the topographic switch.

3. Results and Discussion

3.1. Cold Embossing

Figure 3 shows optical micrographs of the micro-mesh, before (A) and after (B) embossing, and of the deformed NiTi substrate (C). The high compression force and the hardness of the NiTi surface have led to the deformation of both, mesh and sample surface. The NiTi sample shows a clear surface deformation in form of a mesh-like pattern. The deformed NiTi surface exhibits a surface pattern with a peak to valley distance of about 11 μm and a width of the grooves between 100 and 200 μm.

The surface topography after planarization is shown in Figure 4. No clear pattern is visible at room temperature (A), after heating the sample up to 80 °C a mesh-like pattern (B) appears on the surface. To test for the switchability and the reversibility, white light interferometry measurements were taken at room temperature, at 80 °C, and again after cooling down to room temperature. Figure 4 shows the topography at room temperature (C), after heating (D), and after cooling down again (E). As soon as the temperature was increased above the phase transformation temperature, a significant mesh-like pattern appeared with structure features of approximately 2–3 μm in height. The average surface roughness R_a increased from 40 ± 6 nm at room temperature to 690 ± 23 nm in the heated state, and recovered to 80 ± 7 nm after cooling back to room temperature. During further heating and cooling cycles, the sample switched reversibly between states (D) and (E).

The switchability and reversibility of the surface structures indicate that embossing a pattern with subsequent re-planarization by a second compression step induces a TWSME. Consequently, a relatively large area may be structured by a simple two-step process in short time compared to single indentations with subsequent grinding. Furthermore, a significant change in the average roughness was measured depending on the sample temperature.

3.2. Pulse Electrochemical Machining

The optical microscopy and SEM images in Figure 5 exhibit the resulting four different sizes of lines and bumps on the NiTi sample surface after the PECM process. Apart from a darker optical appearance due to oxide formation, the space between the protrusions is smooth and non-structured; a clear separation of structured and unstructured area was achieved proving that plastic deformation was highly localized and defined.

The SEM images suggest that the definition of edges of the protrusions formed decreases with decreasing feature size.

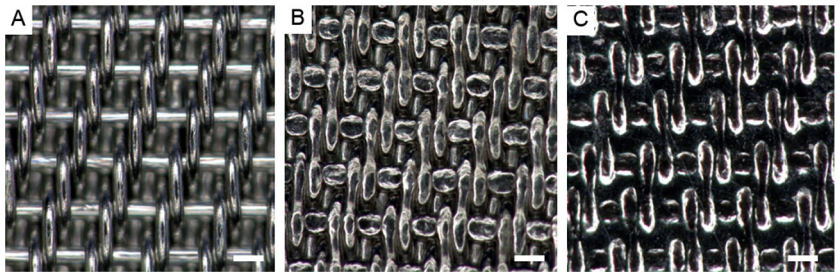

Fig. 3. The images of the cold embossing preparation steps were taken by 3D-optical microscopy and show (A) the metallic micro-mesh before embossing, (B) the micro-mesh after embossing, and (C) the corresponding surface deformation of the NiTi sample. The scale bar corresponds to 100 μm.

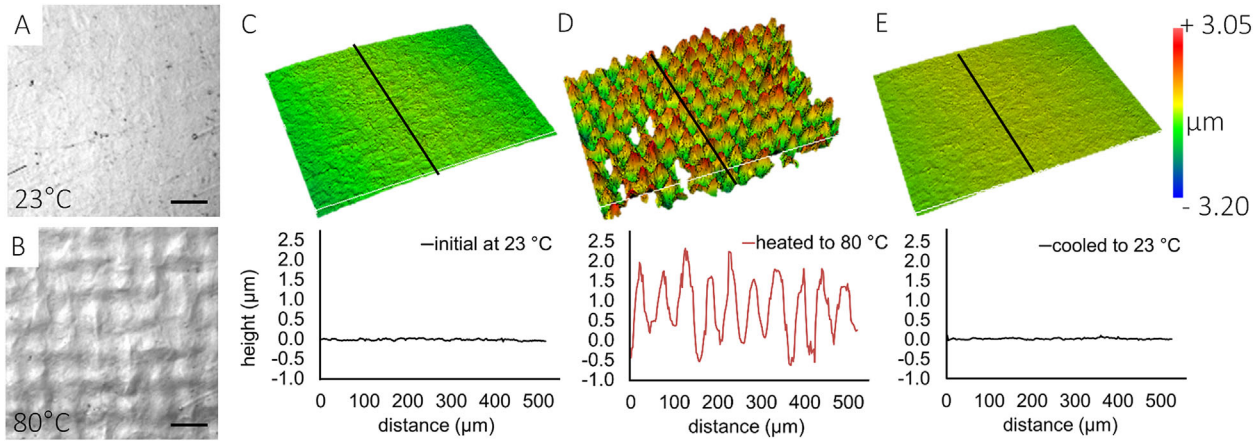

Fig. 4. Optical micrographs and White light interferometry of switchable topography using cold embossing. (A) and (C) correspond to the embossed and re-planarized surface at room temperature, (B) and (D) exhibit the appearing mesh structure upon heating to 80 °C. (E) Demonstrates the recovered flat surface after cooling back to room temperature. The cross-section profiles (black line) of the three different topographies are shown below. The scale bar corresponds to 100 µm.

The edges of the smallest protrusions are hardly visible and their dimensions are difficult to determine. More precise information on the dimensions of the protrusions was obtained by white light interferometry measurements on the switchable TWSME protrusions in the heated state, and on the counterpart structure of the cathode (Table 1).

The measurements show that the lines formed range from 26 ± 3 to 190 ± 4 µm in height and from 207 ± 36 to 608 ± 5 µm in width. The bumps range from 8 ± 1 to 247 ± 4 µm in height and from 372 ± 5 to 1198 ± 12 µm in width.

For better comparability of the PECM structuring accuracy, a form deviation Δl is defined as

$$\Delta l = \frac{|l_s - l_c|}{l_c} \quad (1)$$

where l_s is the length of the cross-section of the structure at the base and l_c is the length of the diameter of the cathode. For $\Delta l = 0\%$, the protrusion exactly matches the diameter of the counterpart in the cathode (Figure 6A).

The results in Figure 6C show that the form deviation increases with decreasing feature size. In most cases, the structures are much larger than their counterpart, reaching values of Δl as high as $190 \pm 24\%$.

The aspect ratio a_s of the structures is defined as

$$a_s = \frac{h_s}{l_s} \quad (2)$$

where h_s is the height of the structure (Figure 6B). The aspect ratios of the protrusions, in this case of the lines and bumps in the four different size categories, are shown in Figure 6D: they decrease with decreasing size from 0.36 ± 0.01 for lines of structure size no. 2 to 0.13 ± 0.03 for size no. 4. Overall, the bumps show a smaller aspect ratio compared to the cross-section of the lines, which was expected because of the low contrast in the SEM and optical microscopy images. Their aspect ratio decreases from 0.26 ± 0.01 to 0.02 ± 0.001.

To explain the deviation between the form of the cathode and the resulting surface pattern, the following aspects have to be considered. The shape evolution on the sample depends on the current density distribution and the mass transport; to achieve a structuring effect also the current distribution on the work piece plays an important role. Therefore, a small gap size and a homogeneous flow of the electrolyte are crucial for precise manufacturing via PECM.[20,23,24] The gap size of the cathode and the NiTi surface slightly increases during the anodization process leading to an ill-defined boundary geometry between the processed and unprocessed areas in the smaller structures. A similar deviation in processing accuracy of grooves with different size in NiTi is shown by Lee et al. using PECM.[19] As shown in Figure 6, the aspect ratios of the formed protrusions decrease with structure size, while a widening of the structures occurs. The variation of structure size and spacing on the same cathode leads to lower current densities for the smaller structures, causing a less precise

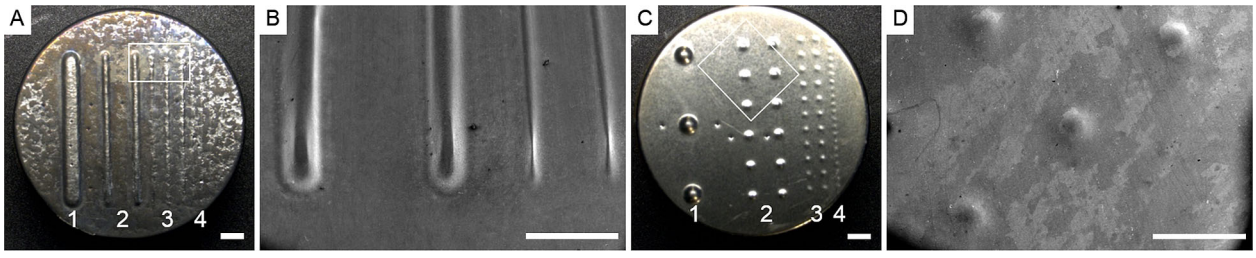

Fig. 5. Optical and SEM micrographs of the surface structures formed by PECM. Lines and semispherical structures were transferred onto the NiTi samples by PECM. (B) and (D) show a close up of the marked section, focusing on the spherical protrusions and the edges of the linear pattern. The scale bar corresponds to 1 mm.

FULL PAPER

Table 1. Dimensions of the cathode structures and the electrochemically processed structures on the NiTi sample: The initial geometries made by PECM are compared to the geometries of the switchable surface structures upon heating the NiTi sample to 80 °C. All data in μm.

Structure no.	Cathode		PECM		Feature at 80 °C	
LINES	Width	Depth	Width	Height	Width	Height
1	500 ± 1	250 ± 1	608 ± 5	190 ± 4	1 341 ± 5	22 ± 4
2	250 ± 1	250 ± 1	310 ± 17	111 ± 10	775 ± 14	4 ± 1
3	150 ± 1	250 ± 1	337 ± 2	49 ± 3	692 ± 15	3 ± 1
4	120 ± 1	250 ± 1	207 ± 36	26 ± 3	368 ± 16	3 ± 1
BUMPS						
1	1 000	1 000	961 ± 18	247 ± 4	1 295 ± 11	9 ± 1
2	500	1 000	806 ± 64	73 ± 1	631 ± 24	3 ± 0.3
3	250	1 000	723 ± 60	15 ± 1	554 ± 29	2 ± 0.2
4	150	1 000	325 ± 5	8 ± 0.4	–	–

material removal in comparison to the larger protrusions.[25] The smaller gap size between the edges of the cathode features and the sample surface leads to stronger anodic dissolution and removal of the sample material than their bottom, with a depth of 500 and 1 000 μm.[20,26] The analysis of form deviation and aspect ratio is a convenient method to characterize the two-way shape-memory effect induced by the compression of surface structures.

Subsequently, the protrusions formed by PECM were compressed into the sample surface using the work piece. As shown in Figure 7, polishing led to an optically smooth, nearly flat surface at room temperature (A and C). During heating up to 80 °C, the specific surface arrays appeared, as shown in Figure 7B and D. After cooling the sample back to room temperature, the arrays disappeared and the surface recovered its optically smooth state. The images in Figure 7

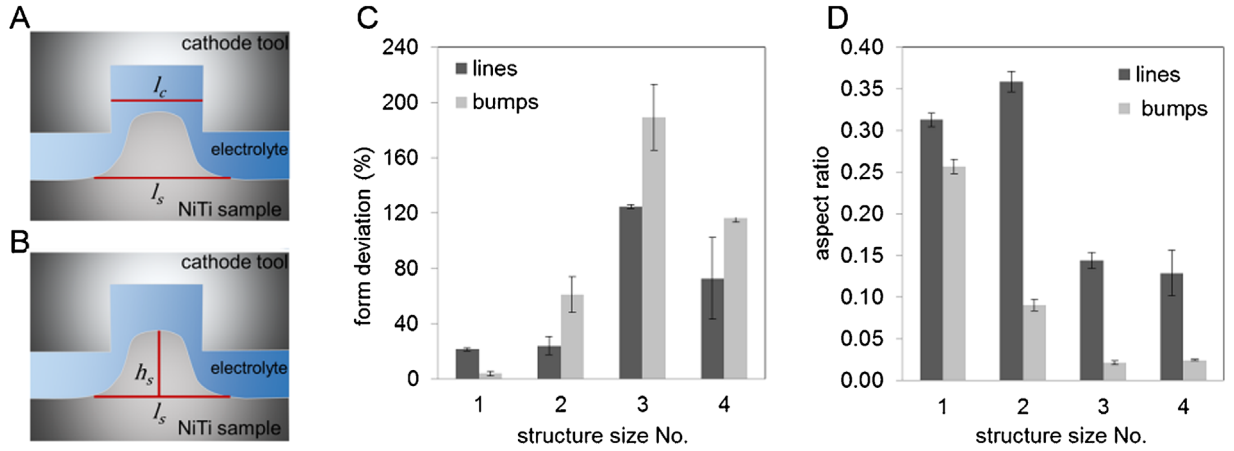

Fig. 6. (A and B) Schematic of interelectrode gap in the PECM process. (C) Form deviation of the lines and semispherical protrusions formed by PECM, listed for each size category. (D) Aspect ratio for the structures made by PECM in each size category.

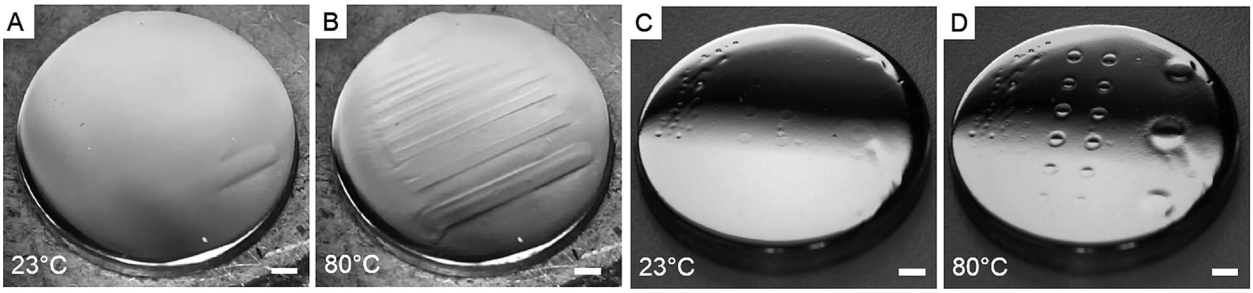

Fig. 7. Optical micrographs showing the switchable topographies. (A and C) The planarized samples at room temperature. (B and D) A change in topography is observed in the heated state. The optically smooth surface shows a linear and spherical pattern. This change in topography can be reversibly switched by temperature cycling. Scale bar 1 mm.

show an exemplary switch of the patterned array after 10 heating and cooling cycles, indicating high reversibility.

Two exemplary white light interferometry measurements of the linear and semispherical protrusions are shown in Figure 8. They confirmed that both geometries deformed reversibly. The height of the two linear structures (Figure 5A No. 3; Figure 8A) increased upon heating from 1.2 to 2.8 μm and 2.4 μm in height and showed a width of 690 and 675 μm. After cooling back to room temperature, the lines recovered their initial profile. The exemplary measurements of the spherical protrusions (Figure 5, C No. 3; Figure 8B) showed a similar behavior. The bump increased from 0.7 to 2.1 μm in height with a width of 561 μm and decreased after cooling to the initial state.

The dimensions of the switchable TWSME protrusions in the heated state at 80 °C are listed for all four size categories in Table 1. Only the smallest bump structures (size No. 4) could not be detected, since no protrusions appeared in the heated state.

An interesting feature to be noted is the lowering of the edge for the spherical protrusions in the heated state, leading to a circular groove around the bump. In the displayed example, the depth of the groove is about 0.7 μm leading to height change of 2.8 μm measured from peak to valley. Thus, upon heating the surface shows two different deformation directions induced by one single compressive pre-deformation.

This effect is not reported in the literature so far and results from the present preparation technique. Due to the compression of material into the surface a complex deformation field is extended underneath, and surrounding, the former PECM structures, which may be considerably more complex than that of a quasi-static indentation. For simplification, we assume that the deformation field resulting from compression of the PECM structures is comparable to that of a flat punch indentation. For this case, Murthy et al. revealed a variation of texture indicating a state of simple shear right at the corner of the flat punch, in our case the edge of the PECM structures.[27] Meanwhile, a state of plane-strain compression was observed directly underneath the flat punch. Applied to our situation, the state of plain-strain will be located centrally below the PECM structure. Based on this, we assume a stagnation of material flow underneath the compressed structures, a presence and orientation of shear bands, and transitions in plastic modes between shear and compression.[27]

The deformation behavior of NiTi shape-memory alloys was shown to be asymmetric in tension and compression, and intrinsic stress fields and defects, which stabilize stress-induced martensite, are considered to be fundamental for the indentation induced TWSME.[28–30] Therefore, it can be assumed that the change in deformation modes below the compressed PECM structures, from plane strain compression to highly strained shear mode, may influence the deformation behavior of the shape-memory alloy.[31] Thus, the presence of two different deformation modes in the area of the compressed PECM structure may have led to different stress fields and defects which induce the bidirectional deformation after the phase transformation.

The induced stress fields result in anisotropic twinning behavior, which is influencing the macroscopic shape change of the surface topography after phase transformation. Regarding the microstructural and thermodynamic findings by Laplanche et al. and Bo and Lagoudas, the complex interaction of microtexture, load direction, and stress-induced formation of martensite plays a crucial role in the switchability of compressed PECM and cold-embossed surfaces.[32–34]

Consequently, the present preparation technique enables the fabrication of switchable surface arrays with a bi-directional extension of protrusions, which is promoted by high strain rates in the dynamic regime and a tailored microstructure.

Having shown that a TWSME can be induced by compression of PECM processed structures, we now compare our results to other studies. Fei et al. reported that the average indentation depth using spherical indenters was 40 times

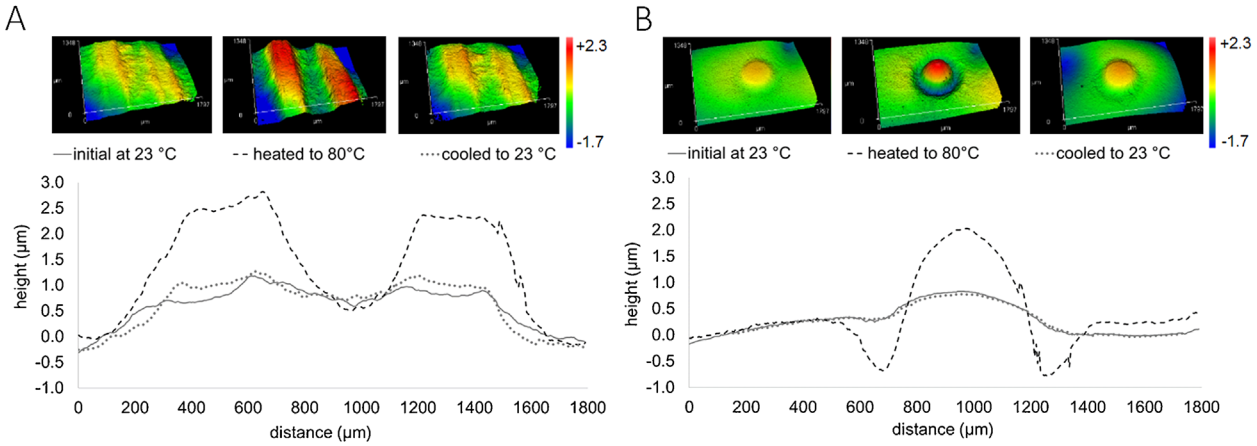

Fig. 8. 3-D topography images and the according cross-section profiles from white light interferometry measurements. An exemplary linear (A) and spherical protrusion (B) are shown for one temperature cycle. Both types of arrays show reversible protrusions which appear in the heated state and recover in the cooled state.

the height of the switchable protrusions obtained by the TWSME.[30] Hence, the height of switchable protrusions was found to be 2.4% of the indentation depth. For comparison we assume, that the height of the structures formed by PECM equals the indentation depth, since the structures should be fully compressed into the surface. Following this assumption, the height of the switchable protrusions was found to range from 3.4 to 14.3% of the indentation depth. This in turn means that a shallower deformation depth is needed to receive the same height of reversible TWSME structures by applying the present technique. Additionally, the surface structuring by PECM followed by compression allows formation of relatively large TWSME arrays at the same time compared to conventional single indentation techniques. Due to the planarization via compression of the structures, less material needs to be removed during the grinding steps. In the present case, one mechanical and chemical polishing step was sufficient to receive an optically smooth surface.

4. Conclusions

This study presents two approaches on the fabrication of switchable surface arrays on NiTi shape-memory alloys. Based on the principle of the indentation induced two-way shape-memory effect, cold embossing and pulsed electrochemical machining with subsequent structure compression, are used to simplify preparation of different reversible surface patterns. In addition, patterning of larger areas at the same time was enabled.

1) The two step process of embossing and re-planarization of a metallic micromesh leads to a reversible change in surface roughness on the micrometer scale with specific geometric features and reversible switching over 10 temperature cycles. This method facilitates the preparation technique for large areas and could enable applications of switchable surface arrays in tribology, switchable adhesion, or biomedicine.[35–37]
2) Pulsed Electrochemical Machining plays in important role in NiTi processing due the oxidation and deformation free formation of complex microstructures without thermal damage or distortion.[38] In the present work, we revealed that a formation of different protruding structures on a NiTi surface was possible via PECM using a tool of holes and grooves.
3) We induced a TWSME by compression of surface structures. After subsequent polishing, arrays with switchable topographies were shown upon heating and cooling the sample above and below its transformation temperatures.
4) Additional to a protruding deformation dimension of the topography, a "sink-in" of the surrounding area – a bidirectional deformation – was observed. Subsequently, two different highly strained regions were induced by the compression of structures, leading to opposite deformation directions during phase transformation. This phenomenon might be attributable to the heterogenic deformation field extending below the PECM structures after compression and the asymmetric deformation behavior of NiTi on compression or shear mode. To confirm these assumptions, a detailed analysis of the microstructure and crystallographic texture in the deformation area has to be conducted.

A fundamental understanding of the factors guiding the different deformation orientations during transformation would enable a more elaborate and coordinated switching of grooves and protrusions.

As mentioned by Zhang et al., a switchable roughness might be of interest for applications in tribology.[9] The surface texture can be varied as a function of temperature, actively by heating above the transformation temperature, or passively, for example, during breaking events using the friction induced heat. The change in surface geometry can then be used to control friction. In addition to the change in topography, the phase transformation itself, from martensite to austenite, may contribute positively to increase wear resistance of the NiTi alloy.[39]

Article first published online: April 4, 2016
Manuscript Revised: March 22, 2016
Manuscript Received: January 8, 2016

[1] K. Otsuka, C. M. Wayman, *Shape Memory Materials*, Cambridge university press, Cambridge **1999**.
[2] J. A. Shaw, S. Kyriakides, *J. Mech. Phys. Solids* **1995**, *43*, 1243.
[3] J. Perkins, *Scr. Metall*. **1974**, *8*, 1469.
[4] K. Otsuka, X. Ren, *Prog. Mater. Sci*. **2005**, *50*, 511.
[5] Y. Zhang, Y. T. Cheng, D. S. Grummon, *Appl. Phys. Lett*. **2006**, *89*, 041912.
[6] Y. Zhang, Y.-T. Cheng, D. S. Grummom, *Surf. Coat. Technol*. **2007**, *202*, 998.
[7] X. L. Fei, Y. J. Zhang, D. S. Grummon, Y. T. Cheng, *J. Mater. Res*. **2009**, *24*, 823.
[8] E. Qin, N. J. Peter, M. Frensemeier, C. P. Frick, E. Arzt, A. S. Schneider, *Adv. Eng. Mater.* **2014**, *16*, 72.
[9] Z. Zhang, D. Zhu, N. Qu, M. Wang, *Microsyst. Technol*. **2007**, *13*, 607.
[10] T. Sun, G. Wang, L. Feng, B. Liu, Y. Ma, L. Jiang, D. Zhu, *Angew. Chem. Int. Ed*. **2004**, *43*, 357.
[11] M. Ebara, *Sci. Technol. Adv. Mater.* **2015**, *16*, 014804.
[12] N. Liu, Q. Xie, W. Huang, S. Phee, N. Guo, *J. Micromech. Microeng*. **2008**, *18*, 027001.
[13] K. Weinert, V. Petzoldt, *Mater. Sci. Eng. A* **2004**, *378*, 180.
[14] K. Weinert, V. Petzoldt, *Mater. Sci. Eng. A* **2008**, *481–482*, 672.
[15] D. Y. Li, *Wear* **1998**, *221*, 116.
[16] J. Jialing, *Acta Metall. Sin*. **1988**, *24*, 66.
[17] O. Weber, H. Natter, D. Bähre, *J. Solid State Electrochem*. **2015**, *19*, 1265.

[18] A. Spieser, A. Ivanov, *Int. J. Adv. Manuf. Technol*. **2013**, *69*, 563.
[19] E.-S. Lee, T.-H. Shin, B.-K. Kim, S.-Y. Baek, *Int. J. Precis. Eng. Manuf*. **2010**, *11*, 113.
[20] M. Kock, V. Kirchner, R. Schuster, *Electrochim. Acta* **2003**, *48*, 3213.
[21] M. Weinmann, in *Naturwissenschaftlich-Technische Fakultät III*, Universität des Saarlandes, Saarbrücken **2014**.
[22] N. Zapp, O. Weber, H. Natter, *Int. J. Electrochem. Sci*. **2015**, *10*, 5434.
[23] C. Rosenkranz, M. M. Lohrengel, J. W. Schultze, *Electrochim. Acta* **2005**, *50*, 2009.
[24] D. Landolt, P. F. Chauvy, O. Zinger, *Electrochim. Acta* **2003**, *48*, 3185.
[25] A. C. West, M. Matlosz, D. Landolt, *J. Electrochem. Soc*. **1991**, *138*, 728.
[26] M. Datta, D. Landolt, *Electrochim. Acta* **2000**, *45*, 2535.
[27] T. G. Murthy, C. Saldana, M. Hudspeth, R. M. Saoubi, Deformation field heterogeneity in punch indentation, presented at *Proceedings of the Royal Society of London A: Mathematical, Physical and Engineering Sciences*, London **2014**.
[28] K. Gall, H. Sehitoglu, *Int. J. Plast*. **1999**, *15*, 69.
[29] M. Frensemeier, E. Arzt, E. Qin, C. P. Frick, A. S. Schneider, *MRS Commun*. **2015**, *5*, 77.
[30] X. Fei, D. S. Grummon, C. Ye, G. J. Cheng, Y.-T. Cheng, *J. Mater. Sci*. **2012**, *47*, 2088.
[31] L. Orgéas, D. Favier, *Acta Mater*. **1998**, *46*, 5579.
[32] Z. Bo, D. C. Lagoudas, *Int. J. Eng. Sci*. **1999**, *37*, 1175.
[33] G. Laplanche, J. Pfetzing-Micklich, G. Eggeler, *Acta Mater*. **2014**, *68*, 19.
[34] A. M. David, C. L. Dimitris, *Smart Mater. Struct*. **2000**, *9*, 640.
[35] W. Ni, Y.-T. Cheng, D. S. Grummon, *Surf. Coat. Technol*. **2006**, *201*, 1053.
[36] M. Frensemeier, J. S. Kaiser, C. P. Frick, A. S. Schneider, E. Arzt, R. S. Fertig, E. Kroner, *Adv. Funct. Mater*. **2015**, *25*, 3013.
[37] M. Ebara, K. Uto, N. Idota, J. M. Hoffman, T. Aoyagi, *Adv. Mater*. **2012**, *24*, 273.
[38] J. J. Maurer, J. L. Hudson, S. E. Fick, T. P. Moffat, G. A. Shaw, *Electrochem. Solid-State Lett*. **2011**, *15*, D8.
[39] L. Yan, Y. Liu, *J. Mater. Res*. **2015**, *30*, 186.

